actuators

MDPI

Article

Synchronous Leveling Control Method of Crane Vehicle Platform Based on Position–Force Coordination

Feixiang Xu [1,2], Haichao Hu [1], Shiyong Feng [1] and Chen Zhou [1,3,*]

[1] School of Information and Control Engineering, China University of Mining and Technology, Xuzhou 221116, China; xufx92@cumt.edu.cn (F.X.); hhc_09@cumt.edu.cn (H.H.); Fsy@cumt.edu.cn (S.F.)
[2] Institute of Electronic and Information Engineering of UESTC in Guangdong, Dongguan 523808, China
[3] State Key Laboratory of Fluid Power & Mechatronic Systems, Zhejiang University, Hangzhou 310027, China
* Correspondence: zc111@cumt.edu.cn

Abstract

Leveling of the crane support platform plays a vital role in operational safety and lifting efficiency; it requires both precise horizontal positioning and the rational distribution of outrigger load. However, the current synchronous leveling methods mainly focus on displacement synchronization leveling while neglecting the control of outrigger load, resulting in the problem of individual outrigger overloading. To address this problem, a synchronous leveling control method with variable load constraints (SLCM-VLC) is proposed in this paper based on the framework of model predictive control. Firstly, the proposed method conducts independent outrigger modeling and decoupling of outriggers through adjacent cross-coupling; then a displacement synchronization controller (DSC) is designed to ensure efficient synchronous leveling. Secondly, a collaborative controller of displacement and force (DFCC) under variable load constraints is designed to overcome the limitations of traditional independent optimization. Subsequently, an extended state observer (ESO) is introduced to compensate for environmental disturbances and control deviations. Finally, the effectiveness of the proposed method is verified through a co-simulation using Matlab, Adams, and Solidworks. The results show that, compared with existing leveling control methods, the proposed method can achieve high precision and rapid leveling under smaller peak load, thereby extending the service life of the platform's electric cylinders.

Keywords: crane outrigger platform; leveling control; synchronization control; outrigger load

check for updates

Academic Editor: Ioan Ursu

Received: 21 July 2025
Revised: 22 August 2025
Accepted: 28 August 2025
Published: 5 September 2025

Citation: Xu, F.; Hu, H.; Feng, S.; Zhou, C. Synchronous Leveling Control Method of Crane Vehicle Platform Based on Position–Force Coordination. *Actuators* **2025**, *14*, 441. https://doi.org/10.3390/act14090441

Copyright: © 2025 by the authors. Licensee MDPI, Basel, Switzerland. This article is an open access article distributed under the terms and conditions of the Creative Commons Attribution (CC BY) license (https://creativecommons.org/licenses/by/4.0/).

1. Introduction

As important engineering machinery equipment, truck cranes have an irreplaceable role in modern industry, construction, and logistics with their strong load-lifting capacity [1–3]. As a crucial part of the truck crane, the level condition and stability of the vehicle-mounted platform are prerequisites for ensuring the lifting capacity and safety of operation [4–7]; these can be improved based on fast and coordinated control of the outrigger. Therefore, it is necessary to study the leveling system to improve the operational efficiency, stability, and safety of the crane.

The leveling of crane outriggers currently mainly relies on manual operation and is not yet fully automated. Current studies in this field predominantly concentrate on the vehicle suspension system and small leveling equipment. For instance, Sun et al. [8] developed an adaptive fuzzy sliding-mode controller (FSMC), achieving high-precision height control of

the suspension system under varying payloads and parameter discrepancies, reducing peak attitude angles, and suppressing oscillations significantly. Li et al. [9] proposed a leveling control method for small leveling equipment based on repetitive positioning, achieving precise leveling for vehicle-mounted theodolites and unloaded outriggers. Although the aforementioned leveling methods can achieve rapid, precise, and reliable leveling of different devices, they are unable to meet the requirements of crane automatic leveling owing to the weak outrigger problem (the outriggers do not bear force or bear little force) and dynamic coupling effects among outriggers. Specifically, as the core issue in crane leveling control, the weak outrigger problem needs to be solved to avoid the risk of crane overturning. On the other hand, the substantial mass of the crane induces an intense dynamic coupling effect among outriggers during leveling. To address these problems, scholars have begun to improve the leveling performance by adopting synchronous leveling control [10,11], achieving global synchronous drive through constructing a coupling model. Owing to its outstanding potential in fully accounting for coupling relationships and the simple structure of the control, a synchronous leveling control strategy is implemented in this paper to enhance the leveling accuracy and speed of the crane.

The aforementioned synchronous leveling control methods focus primarily on the coordination and adjustment of outrigger displacement while neglecting the interaction force between the outriggers and the ground [12]. Notably, an individual outrigger actuator with sustained overload may severely impact the operational efficiency and structural safety of the electric cylinder on it [13]. To overcome this problem, some scholars have studied related explorations in the field of position–force cooperative control in the last few years. For instance, Wang et al. [14] designed a dual-loop attitude control system, where the outer loop achieves automatic leveling and the inner loop realizes force tracking to achieve smooth leveling of the tracked tractor's body. Wu et al. [15] developed an optimal load distribution algorithm based on attitude leveling, whose effectiveness was validated on multi-axle low-speed vehicles. However, the significant structural variations of the crane, the complex working conditions, and the severe load fluctuations make it difficult to quantify the change of outrigger load caused by the variation in the outrigger position, which results in existing methods being unable to adapt to outrigger load control effectively. Furthermore, as a typical underactuated system [16,17], unknown disturbance, multivariable coupling caused by high-order interactions [18], and model uncertainties [19] have a harmful influence on leveling control, but the existing synchronous leveling control methods are unable to deal with these problems effectively.

Recently, benefiting from its unique integrated architecture of prediction, optimization, and feedback, model predictive control (MPC) possesses the strong ability of multi-variable optimization and anti-interference capabilities. Meanwhile, MPC has the flexibility to set model constraints and custom optimization weights. Therefore, compared with other control methods, MPC is more likely to achieve high-precision control while maintaining strong robustness, and this shows a significant potential in multi-variable coupling systems with disturbances such as the cranes. Secondly, when facing the complex nonlinear problems and system uncertainties that occur during the operation of the cranes, fuzzy control methods such as the Mamdani type, T-S type, or data-driven type are adopted. The nonlinear and uncertainties are handled through language or mathematical rules [20,21], updating the weight distribution between outrigger displacement and the load dynamically. This process can achieve real-time optimization of the load constraints and further enhance the robustness of the control system.

In conclusion, aiming at the specific requirements for the synchronous leveling of crane outriggers and their load constraints, a synchronous leveling control method with variable load constraints (SLCM-VLC) is designed in this paper. It has a three-layer

progressive control architecture built upon dual-layer model predictive control, which takes full consideration of the decoupling synchronization, dynamic weighted collaboration, and disturbance compensation [22]. The main contributions of this paper lie in the following aspects: (1) The coupling outriggers are modeled and decoupled independently through adjacent cross coupling. Based on which, a displacement synchronization controller (DSC) is implemented to achieve efficient synchronous leveling of the four-outrigger platform. (2) Based on the proposed SLCM-VLC method, a collaborative controller of displacement and force (DFCC) is designed to achieve the co-optimization of synchronization precision and outrigger force constraint, in which fuzzy control theory (FC) is used to dynamically update the weight of the outrigger load term, overcoming the limitation of traditional strategies that rely on independent optimization. (3) An extended state observer (ESO) is designed to compensate for control deviations caused by environmental disturbances and inaccuracies of the dual-layer MPC model. (4) Comprehensive simulations of the crane outrigger platform are conducted to verify the effectiveness of the proposed method based on the co-platforms of Soildworks, Adams, and Matlab. The experiment results demonstrate that the proposed method not only realizes fast and smooth synchronous leveling of crane outriggers but also improves the service life of the electric cylinder on the outrigger.

The structure of the rest of this paper is as follows. Section 2 models the four-outrigger support platform and leveling mechanism of the crane. In Section 3, the SLCM-VLC method is proposed, and then the DSC, DFCC, and ESO are designed in turn. Section 4 conducts a multi-domain joint simulation and results analysis. Section 5 summarizes the work of this paper.

2. Modeling of Four-Outrigger Support Platform

The three-dimensional model of the truck crane platform is shown in Figure 1a, which consists of vehicle body and outriggers symmetrically arranged at four corners. It can be seen that a rectangular support surface with transverse span of 5000 mm and longitudinal span of 6000 mm is formed based on four outriggers. The leveling and lifting functions of the platform are realized through the electric cylinder integrated in each outrigger.

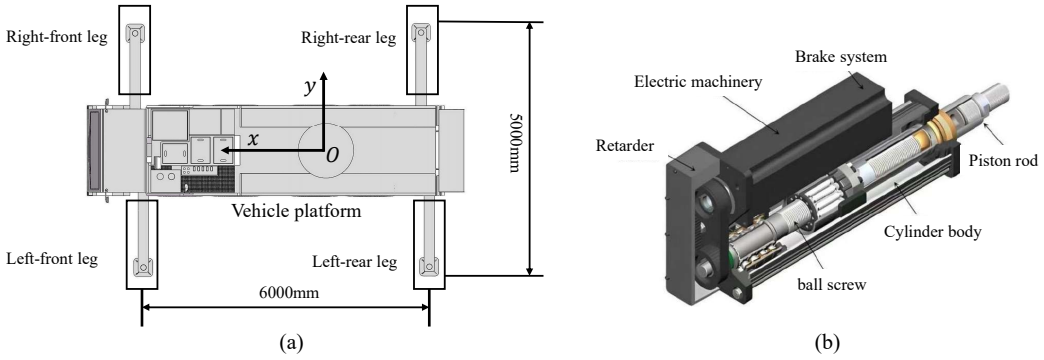


Figure 1. Structure diagram of four-outrigger support platform and electric cylinder: (**a**) the 3-D model of the truck crane platform; (**b**) the internal structure of the outrigger electric cylinder.

Figure 1b illustrates the internal structure of the outrigger electric cylinder, comprising four primary components: the driving mechanism, the deceleration device, the transmission mechanism, and the cylinder body. The drive mechanism generates rotational power through a surface-mounted permanent magnet synchronous motor (PMSM), while the output torque is amplified through a reduction gearbox. Subsequently, the transmission system converts this rotary motion into linear displacement via a ball screw mechanism, thus enabling telescopic actuation of the outrigger. An accurate mathematical model is the

foundation for high-precision leveling control of the crane. Thus, the model of the PMSM and electric cylinder are introduced in the following Sections.

2.1. Mechanism Modeling of Four-Outrigger Support Platform

As the key control variable for the leveling controller, the displacement calculation of each outrigger is the basis for the control strategy design. Therefore, the theory of attitude change and the highest point horizontal measurement method are adopted to calculate the leveling displacement required for the outriggers [23].

To facilitate the calculation and analysis, the truck crane is simplified as a four-outrigger support platform with length of L and width of b. Furthermore, the platform is regarded as being rigid, and the symmetry center of the platform is taken as the origin O. Thus, the rotation diagram of the four-outrigger support platform in a Cartesian coordinate system are shown in Figure 2.

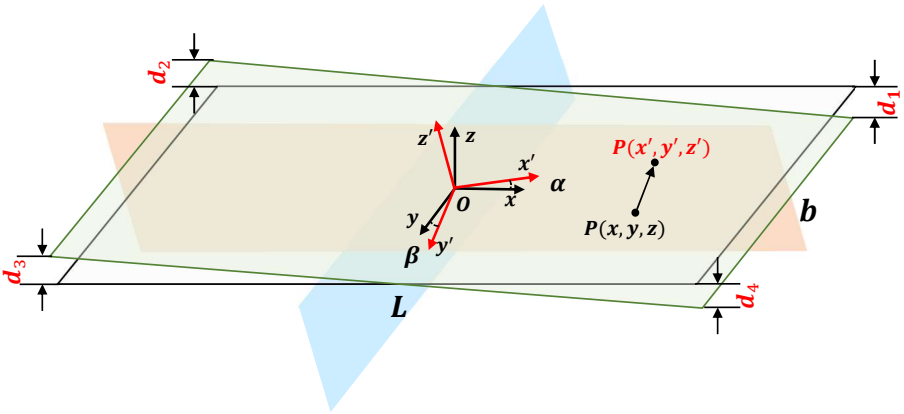


Figure 2. Schematic diagram of four-outrigger support platform.

With the rotation of the platform, inclination angle is composed of pitch angle α around the *x-axis* and roll angle β around the *y-axis*. Suppose that when the outrigger platform is tilted, the position of point P on the platform changes from $P(x, y, z)$ to $P'(x', y', z')$, which can be obtained according to the theory of attitude change.

$$\begin{pmatrix} x' \\ y' \\ z' \end{pmatrix} = \begin{pmatrix} 1 & 0 & 0 \\ 0 & \cos\alpha & -\sin\alpha \\ 0 & \sin\alpha & \cos\alpha \end{pmatrix} \begin{pmatrix} \cos\beta & 0 & \sin\beta \\ 0 & 1 & 0 \\ -\sin\beta & 0 & \cos\beta \end{pmatrix} \begin{pmatrix} x \\ y \\ z \end{pmatrix} \tag{1}$$

Since leveling only considers the vertical displacement, the coordinates of each outrigger in the x-y plane are substituted into Equation (2). Consequently, the vertical displacement d_i $(i = 1 \sim 4)$ for each support outrigger can be obtained as follows:

$$d_i = z_i' - z_i = \frac{-\cos\alpha\sin\beta x_i + \sin\alpha y_i}{\cos\alpha\cos\beta} \ (i = 1 \sim 4). \tag{2}$$

After calculating the vertical displacement of each outrigger, various leveling approaches can be implemented, including the highest point chasing method, the lowest point chasing method, and angle error control leveling method. In this paper, the highest point chasing method with unidirectional extension is applied. Assuming the fourth outrigger represents the highest point, the corresponding momentum of each outrigger is obtained, as displayed in Equation (3):

$$\Delta d = (d_4 - d_1, d_4 - d_2, d_4 - d_3, 0)^T. \tag{3}$$

2.2. Mechanical Model of Electric Cylinder

As the driving source of the outrigger electric cylinder, the following assumptions are made for the PMSM to facilitate modeling and analysis:

(1) Magnetic circuit saturation, eddy current, and hysteresis loss are ignored.

(2) There is no damping winding or damping effect in the rotor and the permanent magnet, respectively.

(3) The back EMF of the motor is sinusoidal, and the distributed magnetomotive forces generated by stator currents in the air gap are also sinusoidal. Thus, the high-order harmonics of the magnetic field should be ignored.

Based on the above assumptions, the mathematical model of the PMSM in the *d-q* rotating coordinate system is obtained as follows [24,25]:

$$\frac{d\omega}{dt} = \frac{1}{J}(T_e - B\omega - T_L) \tag{4}$$

$$\frac{di_q}{dt} = \frac{1}{L_q}(u_q - Ri_q - n_p\omega L_d i_d - n_p\omega\psi) \tag{5}$$

$$\frac{di_d}{dt} = \frac{1}{L_d}(u_d - Ri_d + n_p\omega L_q i_q) \tag{6}$$

$$T_e = \frac{3}{2}n_p[\psi i_q + (L_d - L_q)i_d i_q] \tag{7}$$

where θ is the mechanical angular displacement of the motor, ω is the mechanical angular velocity, T_e represents the electromagnetic torque, B indicates the viscous friction coefficient, T_L is the load torque, J is the rotor moment of inertia, u_q and u_d denote the stator voltages of the *q-axis* and *d-axis*, respectively, i_q and i_d are the stator current under the *d-q axis*, L_q and L_d represent the inductance under the rotating coordinate system in the *d-q* frame, R is the stator resistance, n_p indicates the pole pair, and ψ is the permanent magnet flux linkage.

Owing to the neglect of magnetic saliency effects in the surface-mounted PMSM, the *d-axis* and *q-axis* inductance satisfy $L_q = L_d$. Consequently, there is no reluctance torque component, and the electromagnetic torque T_e is generated solely by the permanent-magnet flux linkage with the current component i_q, as defined in Equation (8). In addition, the reference of the *d-axis* current is usually set to zero ($i_d^* = 0$) in the *d-q* frame, except in the field-weakening region. Given a well-designed current controller, i_d is expected to follow $i_d^* = 0$. Under these assumptions, T_e can be approximated by Equation (8):

$$T_e = \frac{3}{2}n_p\psi i_q \tag{8}$$

Combining Equation (4) and Equation (8), the speed of the motor can be obtained as follows:

$$\dot{\omega} = \frac{1}{J}(\frac{3}{2}n_p\psi i_q - B\omega - T_L) \tag{9}$$

The angular velocity output by the motor serves as the input of the mechanical transmission part, and the actual displacement x_{out} of the electric cylinder is the output of the mechanical transmission part. As a result, the electric cylinder can be modeled as follows:

$$\omega_{sr} = K_{sr}\omega \tag{10}$$

$$v_{out} = \frac{\omega_{sr}p}{2\pi} \tag{11}$$

$$x_{out} = \int_{t_0}^{t_e} v_{out}\,dt \tag{12}$$

where K_{sr} is the reduction ratio of the reducer, ω_{sr} indicates the angular velocity of the screw, p represents the lead of the screw, v_{out} and x_{out} are the output speed and output displacement of the electric cylinder, respectively. t_0 and t_e represent the starting time and stop time of the electric cylinder.

2.3. Collaborative Model of Four-Outrigger Support Platform

The crane outriggers are driven by the electric cylinder installed on each of them, realizing the extension and contraction movement. Combining Equation (4) and Equations from Equation (7) to Equation (12), it is obvious that the angular velocity output by the motor serves as the input of the mechanical transmission part. The mathematical model of the entire electric cylinder is established through integrating the motor and the mechanical transmission, and the state equation of the system is integrated as follows:

$$\dot{x} = Ax + Bu \tag{13}$$

where

$$x = \begin{bmatrix} \omega & x_{out} \end{bmatrix}^T, u = \begin{bmatrix} i_q & T_L \end{bmatrix}^T, A = \begin{bmatrix} -\frac{B}{J} & 0 \\ \frac{P}{K_{sr}\pi} & 0 \end{bmatrix}, B = \begin{bmatrix} \frac{3}{2}n_p\psi & -\frac{1}{J} \\ 0 & 0 \end{bmatrix} \tag{14}$$

The kinematic equation of the whole crane platform is obtained by combining the four electric cylinders.

$$\begin{pmatrix} \dot{x}_1 \\ \dot{x}_2 \\ \dot{x}_3 \\ \dot{x}_4 \end{pmatrix} = \begin{pmatrix} A_1 & & & \\ & A_2 & & \\ & & A_3 & \\ & & & A_4 \end{pmatrix} \begin{pmatrix} x_1 \\ x_2 \\ x_3 \\ x_4 \end{pmatrix} + \begin{pmatrix} B_1 & & & \\ & B_2 & & \\ & & B_3 & \\ & & & B_4 \end{pmatrix} \begin{pmatrix} u_1 \\ u_2 \\ u_3 \\ u_4 \end{pmatrix} \tag{15}$$

where $A_i, B_i (i = 1 \sim 4)$ are the coefficient matrix of each electric cylinder state equation.

To facilitate calculation and analysis, the continuous motion model of the outriggers presented in Equation (15) can be abstracted as follows:

$$\dot{x} = f(x, u) \tag{16}$$

where x is the state vector, u is the action vector, and f is the dynamic function of the electric cylinder.

Due to outstanding forecast performance of MPC, the SLCM-VLC controller designed in this paper is constructed based on the frame of it. Owing to the inherent characteristics of the MPC, which is exclusively applicable to discrete systems, it is necessary to discretize the continuous system. Thus, the discretized equation can be obtained using the forward ruler method.

$$\begin{cases} x_{k+1} = x_k + f(x_k, u_k) \cdot \Delta T = A_d x_k + B_d u_k \\ A_d = E + \Delta T \cdot A, \\ B_d = \Delta T \cdot B \end{cases} \tag{17}$$

where k represents the value of the current moment, ΔT is the discrete time step, A_d and B_d are the corresponding coefficient matrix of x_k and u_k, respectively, E is unit matrix.

Then, in order to achieve the cooperative of the displacement–force dynamic, the Equation (17) can be augmented with electromagnetic torque, and the collaborative modeling of the four-outrigger support platform is completed as follows:

$$\begin{pmatrix} x_{k+1} \\ T_{e,k+1} \end{pmatrix} = \begin{pmatrix} A_d & 0 \\ 0 & 0 \end{pmatrix} \begin{pmatrix} x_k \\ T_{e,k} \end{pmatrix} + \begin{pmatrix} B_d & 0 \\ \frac{3}{2}n_p\psi & 0 \end{pmatrix} \begin{pmatrix} i_q \\ T_L \end{pmatrix} = A_u x_{k,add} + B_u u_k \tag{18}$$

$$\begin{pmatrix} x_{k+1,add_1} \\ x_{k+1,add_2} \\ x_{k+1,add_3} \\ x_{k+1,add_4} \end{pmatrix} = diag_{4\times4}(A_u) \begin{pmatrix} x_{k,add_1} \\ x_{k,add_2} \\ x_{k,add_3} \\ x_{k,add_4} \end{pmatrix} + diag_{4\times4}(B_u) \begin{pmatrix} u_{k,1} \\ u_{k,2} \\ u_{k,3} \\ u_{k,4} \end{pmatrix} \tag{19}$$

At the discrete-time step $k > 0$, based on the Equation (19), the derivation of the MPC's prediction of the future state and output variables of the system in the prediction time domain is as follows:

$$\begin{cases} x_{p,k+1|k} = A_p x_{p,k} + B_p u_{p,k} \\ x_{p,k+2|k} = A_p x_{p,k+1|k} + B_p u_{p,k+1|k} = A_p^2 x_{p,k} + A_p B_p u_{p,k} + B_p u_{p,k+1|k} \\ \vdots \\ x_{p,k+N_p|k} = A_p^{N_p} x_{p,k} + A_p^{N_p-1} B_p u_{p,k} + A_p^{N_p-2} B_p u_{p,k+1|k} + \cdots + A_p^{N_p-N_c} B_p u_{p,k+N_c-1} \end{cases} \tag{20}$$

$$\begin{cases} x_{p,k} = \left(x_{k,add_1}, x_{k,add_2}, x_{k,add_3}, x_{k,add_4}\right)^T \\ u_{p,k} = \left(u_{k,1}, u_{k,2}, u_{k,3}, u_{k,4}\right)^T \\ A_p = diag_{4\times4}(A_u), B_p = diag_{4\times4}(B_u) \end{cases}$$

By organizing Equation (20), the prediction model of MPC can be obtained as

$$\begin{pmatrix} x_{p,k+1} \\ x_{p,k+2} \\ x_{p,k+3} \\ \vdots \\ x_{p,k+N_p} \end{pmatrix} = \begin{pmatrix} B_P & 0 & 0 & \cdots & 0 \\ A_P B_P & B_P & 0 & \cdots & 0 \\ A_P^2 B_P & A_P B_P & B_P & \cdots & 0 \\ \vdots & \vdots & \vdots & \vdots & \vdots \\ A_P^{N_p-1} B_P & A_P^{N_p-2} B_P & A_P^{N_p-3} B_P & \cdots & A_P^{N_p-N_c} B_P \end{pmatrix} \begin{pmatrix} u_{p,k} \\ u_{p,k+1} \\ u_{p,k+2} \\ \vdots \\ u_{p,k+N_c-1} \end{pmatrix} + \begin{pmatrix} A_P \\ A_P^2 \\ A_P^3 \\ \vdots \\ A_P^{N_p} \end{pmatrix} \begin{pmatrix} x_{p,k} \\ x_{p,k+1} \\ x_{p,k+2} \\ \vdots \\ x_{p,k+N_p-1} \end{pmatrix}, \quad \begin{cases} x_{p,k} = \left(x_{k,add_1}, x_{k,add_2}, x_{k,add_3}, x_{k,add_4}\right)^T \\ u_{p,k} = \left(u_{k,1}, u_{k,2}, u_{k,3}, u_{k,4}\right)^T \\ A_p = diag_{4\times4}(A_u), B_p = diag_{4\times4}(B_u) \end{cases} \tag{21}$$

3. Design of Synchronous Leveling Control Strategy

3.1. Overall Structure of SLCM-VLC Control Strategy

Following the collaborative model construction in Section 2, a SLCM-VLC control strategy based on the MPC frame is proposed. This strategy incorporates a multi-step prediction and rolling optimization mechanism, aiming to enhance dynamic response performance and anti-interference capabilities. In the design phase, the inclination angle of the vehicle platform, the synchronization error among outriggers, the load variation of the outriggers, and the dynamic performance of the electric cylinder are considered as the core indicators and input parameters to co-optimize outrigger position–force performance. The overall structure is shown in Figure 3.

It can be seen that the SLCM-VLC consists of three parts: displacement synchronization controller (DSC), collaborative controller of displacement and force (DFCC), and compensation scheme of uncertainty-oriented outrigger (CSU). The DSC is applied to deal with the synchronization problem of the crane outrigger displacement with consideration of the adjacent cross-coupling relationships among the four outriggers. And the DFCC achieves the coordination of the outrigger load and position through updating the weight

dynamically. Moreover, the ESO is introduced in the CSU to compensate the modeling error and the external uncertainty of the crane outrigger platform.

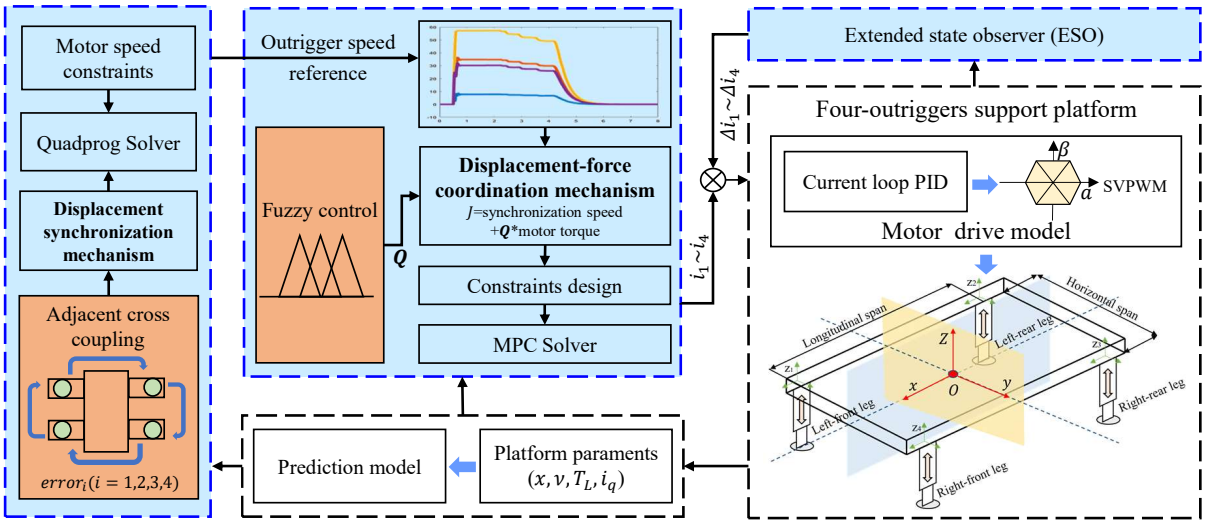


Figure 3. Structure of the SLCM-VLC control strategy.

3.2. Displacement Synchronization Controller

As mentioned in Section 2, a synchronous leveling control strategy based on adjacent cross-coupling is implemented in this paper to enhance the leveling accuracy and speed of the crane. The core principle of adjacent cross coupling control is that coupling errors are derived from position error. As a result, a synchronization cost function that integrates coupling errors is designed to convert the ideal displacement of the outriggers into a matching synchronous reference velocity, providing a reference for the collaborative optimization of the DFCC. The optimization objectives mainly include the synchronization error among the platform's outriggers and the variation increment of the control input so as to ensure the synchronous leveling and smooth operation of the system. The specific design of the cost function in displacement synchronization controller is introduced as follows:

Firstly, considering the tracking accuracy of the outriggers to the ideal displacement $x_{ref,i}$ $(i = 1 \sim 4)$, the cost function is designed accordingly to minimize the cumulative tracking error in the prediction time domain.

$$J_1 = \sum_{m=0}^{N_p-1} \left\| \begin{pmatrix} x_{out,1}(k+m|k) \\ x_{out,2}(k+m|k) \\ x_{out,3}(k+m|k) \\ x_{out,4}(k+m|k) \end{pmatrix} - \begin{pmatrix} x_{ref,1}(k+m|k) \\ x_{ref,2}(k+m|k) \\ x_{ref,3}(k+m|k) \\ x_{ref,4}(k+m|k) \end{pmatrix} \right\|^2_{Q_e} \tag{22}$$

$$x_{out,i} = \begin{bmatrix} 0 & 1 & 0 \end{bmatrix} \cdot x_{k.add_i} \quad (i = 1 \sim 4)$$

where N_p is the prediction time domain, i represents the future time domain, Q_e is the weight matrix of the trajectory tracking error, and the maximum value of x_{ref} is set to 610 mm.

Then, the reference trajectory is matched with the velocity of the reference on the basis of the cross-coupling. Unlike the conventional synchronization strategies that track with the same displacement, the ideal telescopic displacement of each outrigger is usually different during the leveling process. Therefore, the synchronous control methods based on the same displacement setting value cannot be directly adopted. For this reason, a synchronization cost function based on relative displacement is designed in this paper.

$$J_2 = \sum_{m=0}^{N_p-1} \left\| \underbrace{\begin{pmatrix} C_1 & -C_2 & & \\ & C_2 & -C_3 & \\ & & C_3 & -C_4 \\ -C_1 & & & C_4 \end{pmatrix}}_{C_{total}} \begin{pmatrix} x_{k+m,add_1} \\ x_{k+m,add_2} \\ x_{k+m,add_3} \\ x_{k+m,add_4} \end{pmatrix} \right\|_{Q_{sy}}^2, C_i = [0 \quad \frac{x_{out,i}}{x_{ref,i}} \quad 0] \ (i = 1 \sim 4) \tag{23}$$

where Q_{sy} is the weight coefficient matrix of the corresponding outrigger synchronization.

Finally, in order to ensure the stability and smoothness of trajectory tracking and outrigger synchronization, it is necessary to consider the variation in the control input u. The cost function of the variation in the control input is designed as follows:

$$J_3 = \sum_{m=0}^{N_c-2} \|(u(k+m+1|k) - u(k+m|k))\|_R^2 \tag{24}$$

where N_c is the control time domain, R is the weight coefficient matrix of the control.

By combining the equations from Equation (22) to Equation (24), the cost function for the displacement synchronization controller is formulated as

$$J = (J_1 + J_{1,m=N_p}) + (J_2 + J_{2,m=N_p}) + J_3 \tag{25}$$

In a word, there is a novel attempt in the design of cost function for the displacement synchronization controller that incorporates adjacent cross-coupling relationships among the four outriggers. Based on the displacement synchronization controller, the ideal displacement of the outrigger is converted into a synchronous reference speed ($v_{1,ref} \sim v_{4,ref}$) through using the Quadprog solver under the constraints of motor parameters and cost function. As a result, the leveling control of the four outrigger displacements is achieved.

3.3. Collaborative Controller of Displacement and Force

Based on the synchronous reference speed obtained from the displacement synchronization controller, this section focuses on position–force coordination and the increment change of the control input as the optimization objectives of the MPC. A collaborative controller is constructed to achieve the coordination of displacement and force. Specifically, a novel cost function which integrates position errors and force constraint terms is constructed, whose design process is summarized as follows.

Firstly, a collaborative cost function in Equation (26) is constructed by integrating the outrigger load optimization term to dynamically coordinate the position synchronization and the load distribution of the outriggers. This improves the performance of the electric cylinder of the crane outriggers, such as service life, load distribution, etc.

$$\begin{aligned} J = & \sum_{m=0}^{N_p-1} \left\| \begin{pmatrix} C_{f_1} & & & \\ & C_{f_2} & & \\ & & C_{f_3} & \\ & & & C_{f_4} \end{pmatrix} \begin{pmatrix} x_{k+m,add_1} \\ x_{k+m,add_2} \\ x_{k+m,add_3} \\ x_{k+m,add_4} \end{pmatrix} - \begin{pmatrix} ref_{1,k+N_p} \\ ref_{2,k+N_p} \\ ref_{3,k+N_p} \\ ref_{4,k+N_p} \end{pmatrix} \right\|_Q^2 \\ & + \left\| \begin{pmatrix} C_{f_1} & & & \\ & C_{f_2} & & \\ & & C_{f_3} & \\ & & & C_{f_4} \end{pmatrix} \begin{pmatrix} x_{k+N_p,add_1} \\ x_{k+N_p,add_2} \\ x_{k+N_p,add_3} \\ x_{k+N_p,add_4} \end{pmatrix} - \begin{pmatrix} ref_{1,k+N_p} \\ ref_{2,k+N_p} \\ ref_{3,k+N_p} \\ ref_{4,k+N_p} \end{pmatrix} \right\|_F^2 \\ & + \sum_{m=0}^{N_c-2} \|(u(k+m+1|k) - u(k+m|k))\|_R^2 \\ & C_f = \begin{bmatrix} 1 & 0 & 0 \\ 0 & 0 & 1 \end{bmatrix}, ref_i = \begin{bmatrix} v_{i,ref} \\ 0 \end{bmatrix} \ (i = 1 \sim 4) \end{aligned} \tag{26}$$

where C_f is the output matrix, F is the terminal weight matrix, and Q is the variable weight matrix, which is divided into speed Q_{speed} and torque Q_{Nm}.

Furthermore, in order to balance the maximum load variation and synchronization effect among outriggers dynamically, and combined with the actual requirements of the crane, the rule design of the fuzzy controller should be directly based on engineering experience or experimental data [21]. This approach provides the intuitive mapping between the load variation and the weight adjustment and reduces the dependency on precise system models to ensure real-time performance. Therefore, this paper employs a real-time and reliable Mamdani fuzzy controller, which contrasts with the complex rule design and strong dependence on mathematical models [20] of the T-S fuzzy controller, as well as the adaptive fuzzy controller that requires online computing resources [20]. The dynamic calculation of the variable weight Q is achieved through this fuzzy controller.

In the designed fuzzy controller, the difference e between the actual and ideal outrigger output torque, along with its change rate Δe, are taken as the two inputs. The weight adjustment factor of the motor torque is set as the output. The fuzzy sets for input and output are defined as NB (negative large), NM (negative medium), NS (negative small), PS (positive small), PM (positive medium), and PB (positive large). Although the inputs and output are non-negative, the fuzzy rules are retained for convenience. The specific fuzzy rules are shown in Table 1.

Table 1. Fuzzy control rules.

Weight		**Torque Error**					
		NB	**NM**	**NS**	**PS**	**PM**	**PB**
Torque error rate	NB	NB	NB	NM	NS	PM	PB
	NM	NB	NM	NS	PS	PM	PB
	NS	NB	NS	PS	PM	PB	PB
	PS	NB	PS	PM	PB	PB	PB
	PM	NB	PM	PM	PB	PB	PB
	PB	NB	PM	PB	PB	PB	PB

Considering the complexity of the dynamics of each outrigger during the leveling process, the Gaussian membership functions with high accuracy and strong adaptability are adopted for both input and output. Based on the fuzzy control rules formulated in Table 1, the designed input and output membership functions are shown in Figure 4.

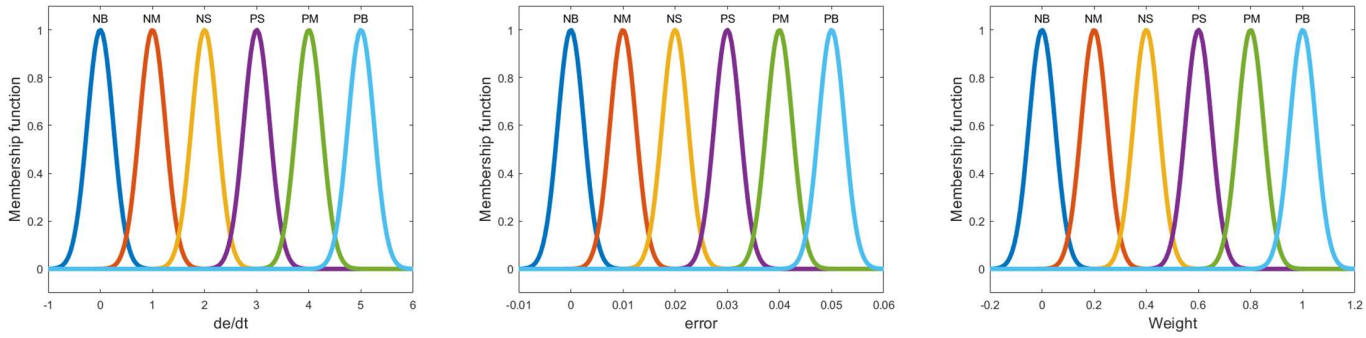


Figure 4. Input and output membership functions.

According to the designed fuzzy rules and membership functions, for each rule (if x_1 is $A_{i,1}$, x_2 is $A_{i,2}$, then y is B_i), the activation degree is calculated as

$$\begin{cases} \mu(x) = \exp(-\frac{(x-c)^2}{2\sigma^2}) \\ \alpha_i = \mu_{A_{i,1}}(x_1) \times \mu_{A_{i,2}}(x_2) \\ \mu_B(y) = \max(\alpha_i \times \mu_{B_{i,1}}(x_1)) \end{cases} \tag{27}$$

where c and σ are the center and standard deviation of Gaussian function, respectively, and α_i represents the activation strength of the fuzzy rules. $\mu_B(y)$ denotes the membership degree of the output variable y to the fuzzy set B.

Using the centroid method for defuzzification, the control output Q_y can be obtained as follows:

$$Q_y = \frac{\int y \cdot \mu_B(y) dy}{\int \mu_B(y) dy} \tag{28}$$

Owing to the physical limitations of the electric cylinder outriggers in the leveling process, it is also necessary to set boundary limits on the maximum speed, speed increment, current amplitude, and current increment of the electric cylinder motor. The constraints on control quantity and control quantity increment are constructed as follows:

$$\begin{cases} u_{\min} \le u(k+m|k) \le u_{\max}, 0 \le m \le N_c - 1 \\ \Delta u_{\min} \le \Delta u(k+m|k) \le \Delta u_{\max}, 0 \le m \le N_c - 2 \end{cases} \tag{29}$$

where $u_{\min}$, $u_{\max}$ are the lower limit and upper limit of the control quantity, respectively, and $\Delta u_{\min}$, $\Delta u_{\max}$ indicate the lower and upper limits of the control increment, respectively.

Finally, under the constraints of actual physical conditions, the final control values ($i_1 \sim i_4$) at the time of k are output based on collaborative controller, realizing the coordination of the outrigger's load and the position.

3.4. Compensation Scheme of Uncertainty-Oriented Outrigger

To compensate for control deviations caused by external environmental disturbances and inaccuracies in the dual-layer MPC model, an ESO is designed.

As shown in Figure 5, the modeling error and the external disturbance are regarded as the total disturbance for real-time estimation and dynamic compensation, and the ESO can observe the displacement output of each outrigger electric cylinder. Then the control signals of the motor current are obtained and integrated with the compensation amounts ($\Delta i_1 \sim \Delta i_4$). Finally, accurate control of the electric cylinder is driven through the motor space vector pulse width modulation (SVPWM), realizing the telescopic movement of the outriggers.

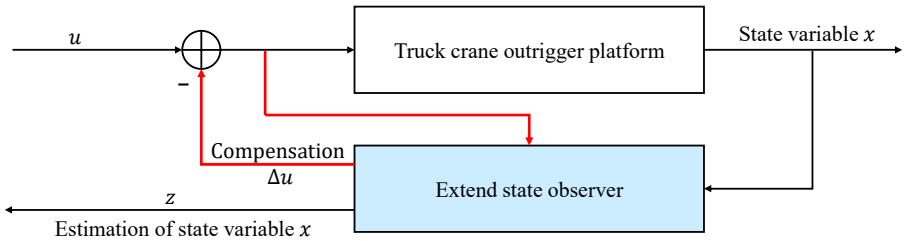


Figure 5. Schematic of the extended state observer.

According to the equations from Equation (12) to Equation (14), the state vector of the ESO is defined as $[x_1 \quad x_2] = [x_{out} \quad \omega]$. The total disturbance is considered as an extended

state $x_3 = f(x_1, x_2, w, t)$. At the same time, assuming the extended state is bounded and differentiable, the expression of the electric cylinder can be written as

$$\begin{cases} \dot{x}_1 = C_t x_2 \\ \dot{x}_2 = bu + f(x_1, x_2, w, t) \\ \dot{x}_3 = f(x_1, x_2, w, t)' \\ y = x_1 \end{cases} \tag{30}$$

where b is the action gain coefficient, C_t is the transmission coefficient of the electric cylinder transmission device, and $C_t = \frac{P}{K_{sr} \cdot 2\pi}$. f represents the total disturbance, including the deterministic term $-\frac{B}{J}\omega - \frac{T_L}{J}$, internal dynamics $f(x_1, x_2, t)$, and external disturbance $w(t)$.

Then, ESO is accordingly designed as

$$\begin{cases} e = \hat{y} - y \\ \dot{\hat{x}}_1 = C_t \hat{x}_2 - \beta_1 e \\ \dot{\hat{x}}_2 = \hat{x}_3 - \beta_2 fal(e, \alpha_1, \delta) + bu \\ \dot{\hat{x}}_3 = -\beta_3 fal(e, \alpha_2, \delta) \end{cases} \tag{31}$$

where e is the output estimation error. $\hat{x}_1, \hat{x}_2, \hat{x}_3, \hat{y}$ are the observed values of x_1, x_2, x_3, y, respectively. $\beta_1, \beta_2, \beta_3$ are the three gain coefficients of the observer, and fal is a nonlinear function to suppress errors, whose expression is

$$fal(e, \alpha, \delta) = \begin{cases} \frac{x}{\delta^{1-\alpha}}, |x| \le \delta \\ sign(x)|x|^{\alpha}, |x| > \delta \end{cases} \tag{32}$$

where α is the nonlinear index, which controls the degree of nonlinearity, and δ is the thickness of the boundary layer for switching.

Regarding the stability of the proposed controller, the analytical approach in [26] is adopted. Firstly, the stability of MPC is rigorously guaranteed through well-documented theoretical proofs. Then, the fuzzy control is used to update the weight value $Q \in [0, 1]$ in the cost function, and the weight update is adjusted by the control target. This dynamic update method does not change the positive definiteness of the cost function, so it will not destroy the stability of the controller.

In order to further prove the stability, the proposed SLCM-VLC can be regarded as a front-to-back series MPC under variable weight for stability proof, and the following joint Lyapunov function V is defined:

$$V = V_1 + V_2 \tag{33}$$

where

$$V_1 = \sum_{m=0}^{N-1} \| [x_{out,i}(k+m \mid k)]_{i=1}^{4} - x_{ref,i}[(k+m \mid k)]_{i=1}^{4} \|_{Q_e}^2 + \| C_{total}[x_{k+m,add_i}]_{i=1}^{4} \|_{Q_{sy}}^2 \tag{34}$$

$$\begin{aligned} V_2 = & \sum_{m=0}^{N-1} \| diag(C_{f_1}, C_{f_2}, C_{f_3}, C_{f_4})[x_{k+m,add_i}]_{i=1}^{4} - [ref_{i,k+m}]_{i=1}^{4} \|_{Q}^2 \\ & + \sum_{m=0}^{N-1} \| diag(C_{f_1}, C_{f_2}, C_{f_3}, C_{f_4})[x_{k+N_p,add_i}]_{i=1}^{4} - [ref_{i,k+N_p}]_{i=1}^{4} \|_{F}^2 \end{aligned} \tag{35}$$

For a discrete system, the differential analysis of the joint Lyapunov function is $\Delta V = \Delta V_1 + \Delta V_2$. Owing to Q_e and Q_{sy} being constant matrices, ΔV_1 is only related to the dynamic changes of x_{out}, x_{ref} and x_{add}. It can be obtained that $\Delta V_1 \le 0$ by referring

to the traditional stability theory. Then, considering the weight Q in V_2 is dynamically updated, the difference term for ΔV_2 is

$$\begin{aligned}\Delta V_2 = &(\left\| diag(C_{f_1}, C_{f_2}, C_{f_3}, C_{f_4})[x_{k+N-1,add_i}]_{i=1}^{4} - [ref_{i,k+N-1}]_{i=1}^{4} \right\|_{Q_{k+1}}^{2}) \\ &-(\left\| diag(C_{f_1}, C_{f_2}, C_{f_3}, C_{f_4})[x_{k+N-1,add_i}]_{i=1}^{4} - [ref_{i,k+N-1}]_{i=1}^{4} \right\|_{Q_k}^{2})\end{aligned} \tag{36}$$

Since the weight change directly affects the difference term of ΔV_2, and the dynamic matrix Q satisfies the degression, convergence, and change rate constraints, the joint Lyapunov function $\Delta V_2 \leq 0$. $\Delta V_1 + \Delta V_2 \leq 0$ can prove that the designed controller is stable.

4. Co-Simulation and Analysis of Synchronous Leveling System

4.1. Simulations in Multi-Domain

To verify the effectiveness of the strategy proposed in this paper, the virtual prototype technology is used to construct the outrigger platform of the truck crane in Soildworks, Adams, and Matlab, as shown in Figure 6. Table 2 displays the parameters of the controller, and the settings of the parameters in the simulation are shown in Table 3.

Table 2. Controller parameters.

Parameters	Value
Sampling time T	0.02 s
Prediction step size (DSC)	50
Prediction step size (DFCC)	10
Control step size (DSC)	5
Control step size (DFCC)	5
Nonlinear index α	0.5
Boundary-layer thickness δ	0.001 mm
ESO gain coefficient $\beta_1, \beta_2, \beta_3$	$3 \times 10^2\,s^{-1}, 3 \times 10^4\,s^{-2}, 3 \times 10^5\,s^{-3}$

Table 3. Parameters setting in simulation.

Parameters	Value
Motor pole pairs n_p	4
Stator resistance R	$0.138 \pm 10\%\,\Omega$
Motor flux linkage ψ	0.11895 Wb
d-axis inductance L_d	628.78 µH
q-axis inductance L_q	628.78 µH
Moment of inertia J	$0.007\ kg \cdot m^2$
Friction coefficient B	$0.003\ N \cdot m \cdot s \cdot rad^{-1}$
Reduction ratio K_{sr}	17.68
Screw outer diameter	100 mm
Screw lead p	16 mm
Maximum stroke of electric cylinder	610 mm
Load of truck crane	40 t
Transverse span	5000 mm
Longitudinal span	6000 mm

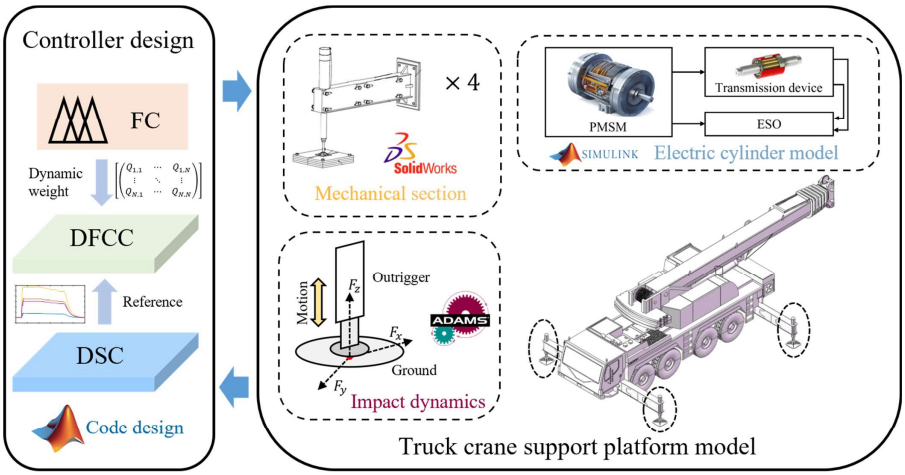


Figure 6. Co-simulation model of synchronous leveling system.

In order to better evaluate the performance of the SLCM-VLC, two working conditions, a flat road and an undulating road, are simulated. The proposed method is applied compared with the classic synchronous algorithm (PID-CC), the model predictive control synchronous algorithm (MPC-CC), the fixed-weight SLCM-VLC, and the SLCM-VLC under the T-S model to conduct a comprehensive assessment. Specifically, the crane's body inclination angle on the flat road is relatively small ($\leq 1°$), while the body inclination angle is set at around 3° on the undulating road to ensure lifting safety. The automatic outrigger leveling operation is simulated under two different working conditions, focusing on core indicators such as the leveling accuracy, the synchronization performance e_{sy}, the variation in the load f_{Load}, and the dynamic performance of the electric cylinder. Among them, the relevant calculation formulas are as follows:

$$e_{sy} = max(\frac{x_{out,1}}{x_{ref,1}}, \frac{x_{out,2}}{x_{ref,2}}, \frac{x_{out,3}}{x_{ref,3}}, \frac{x_{out,4}}{x_{ref,4}}) - min(\frac{x_{out,1}}{x_{ref,1}}, \frac{x_{out,2}}{x_{ref,2}}, \frac{x_{out,3}}{x_{ref,3}}, \frac{x_{out,4}}{x_{ref,4}}) \tag{37}$$

$$f_{Load} = \frac{Load_{max} - Load_{static}}{Load_{static}} \tag{38}$$

where x_{out} andx_{ref} are, respectively, the output displacement and the ideal displacement of the outrigger electric cylinder, $Load_{max}$ is the maximum outrigger load, and $Load_{max}$ represents the static outrigger load.

4.2. Analysis of Simulation Results

4.2.1. Analysis of Simulation Results on the Flat Road

Figure 7 demonstrates the trajectory tracking and synchronous performance of each outrigger under the proposed SLCM-VLC method. It can be seen that all outriggers can extend ideal displacement synchronously within 6 s without overshoot.

The pitch angle and the roll angle of the vehicle platform during leveling process are shown in Figure 8. It can be seen from Figure 8a,b that both the pitch angle and roll angle can reach a safe range of 0.1° within 4.23 s based on the proposed SLCM-VLC and then further converge the angle to around 0° finally. These indicate that the proposed SLCM-VLC can achieve high-precision synchronous leveling with a fast speed.

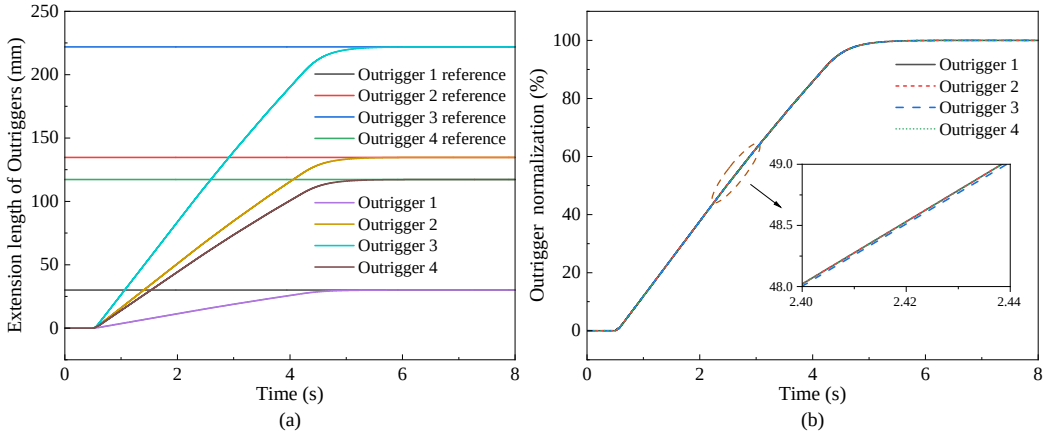


Figure 7. Displacement of outrigger: (**a**) trajectory tracking; (**b**) synchronization performance.

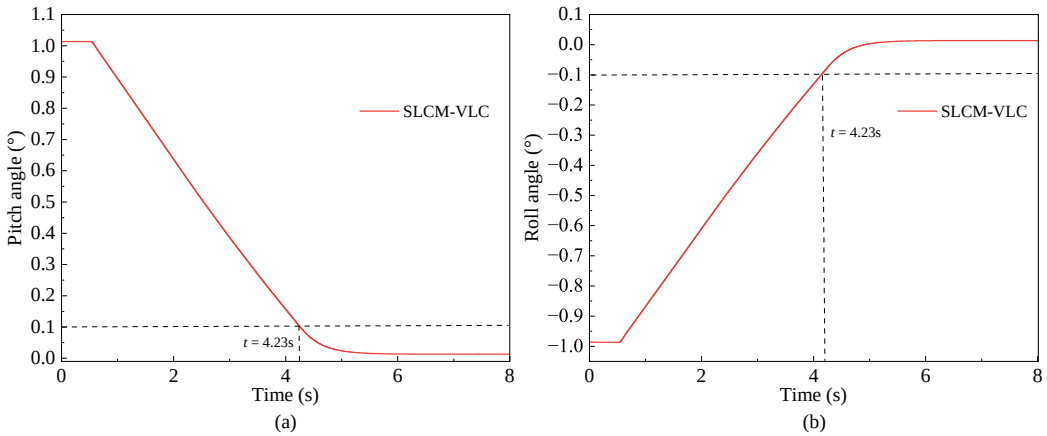


Figure 8. Position of vehicle platform on the flat road: (**a**) pitch angle variation; (**b**) roll angle variation.

As shown in the relative synchronization error in Figure 9, during the startup stage of the synchronous leveling from 0 s to 1 s, there is a sudden change in the synchronization error of four outriggers under PID-CC, with the peak error reaching as high as 0.70% and a convergence lag of nearly 1 s. In contrast, the other four methods suppress the peak of the relative synchronization error to approximately 0.40% and rapidly converged the error to around 0 within 0.3 s, which can be attributed to the unique rolling optimization capability of the MPC framework. As leveling progresses, the proposed SLCM-VLC and SLCM-VLC(T-S) exhibit the most significant fluctuations between 2 s and 5 s and then rapidly converge to zero. This abnormal state is caused by the change of the synchronization matrix attributing to the displacement–force coordination mechanism of the DFCC as a result of balancing the synchronization error and the load on outriggers, which will be further analyzed in subsequent Figure 10.

According to the initial pitch angle 1° and the initial roll angle −1°, it can be seen that outrigger 3 (right rear outrigger) is the lowest point and outrigger 1 (left front outrigger) is the highest point, resulting in significant spatial differentiation of the load among the outriggers. Compared with the controller under the traditional method, fixed weight, and the T-S type, it can be observed from Figure 10 that the proposed SLCM-VLC suppresses the load fluctuation on outrigger 1 and outrigger 3 from 2 s to 5 s, reducing the maximum load significantly. And the load of outrigger 2 and outrigger 4 only increases a little, owing to the dynamic coupled characteristics among the four outriggers. This phenomenon not only verifies the effectiveness of the proposed load constraint mechanism (fuzzy control real-time update) but also explains the reason for the significant fluctuation in the synchronization error in Figure 9. Specifically, the partial synchronization error is sacrificed in exchange for

significant load reduction, which realizes the balance of the synchronous leveling and the load of the outrigger.

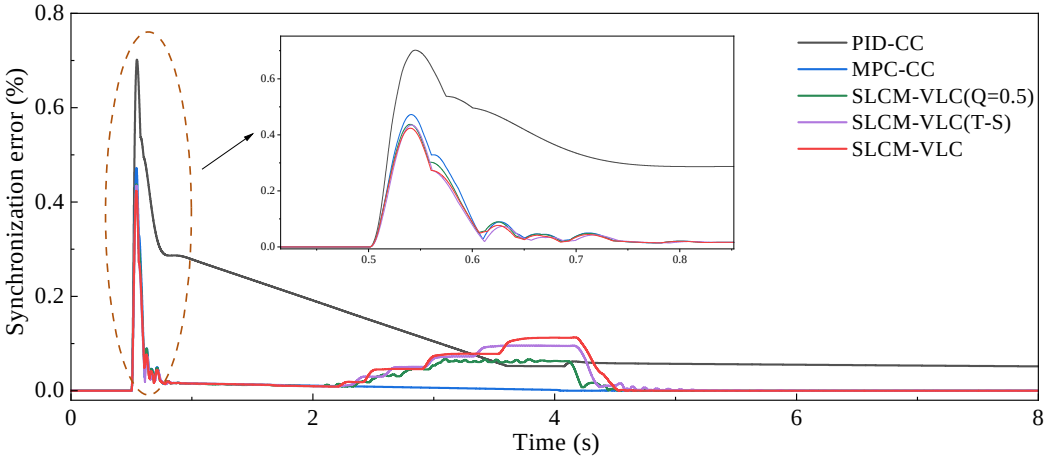


Figure 9. Comparison of relative synchronization error on the flat road.

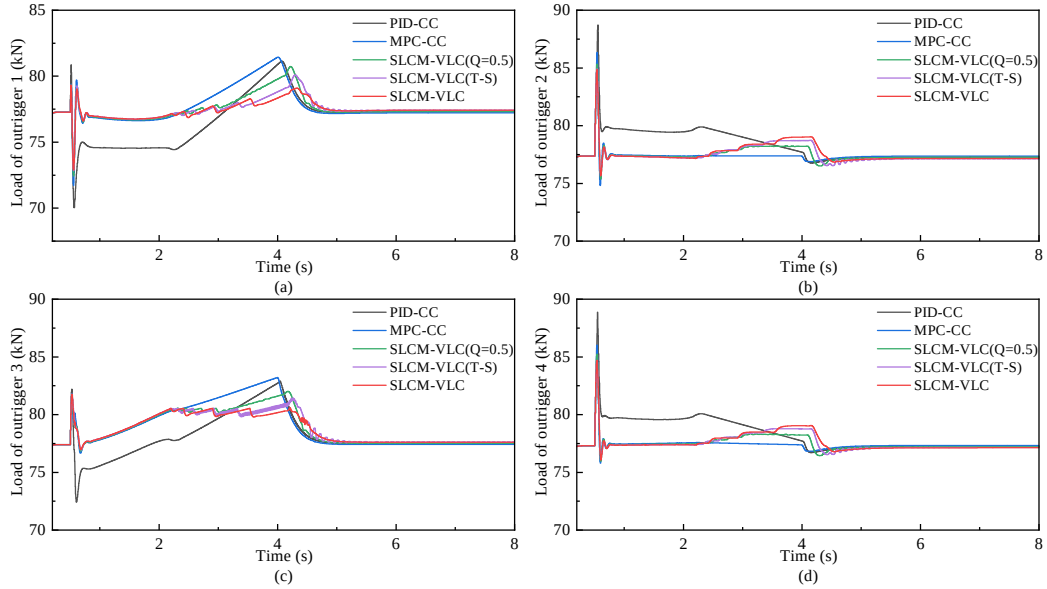


Figure 10. Load variations of each outrigger on the flat road: (**a**) outrigger 1; (**b**) outrigger 2; (**c**) outrigger 3; (**d**) outrigger 4.

Meanwhile, compared with the SLCM-VLC method of the T-S fuzzy controller type, equivalent force constraint performance is achieved. However, owing to its high dependency on precise mathematical models, the type T-S exhibits the load's oscillatory behavior caused by the rapid change in weight Q. In contrast, the proposed method employs Gaussian membership functions and empirically validated rules, demonstrating the efficiency and reliability of the embedded fuzzy controller. In order to conduct a more intuitive analysis, specific statistical analysis data are shown in Table 4.

As presented in Table 4, the static load of each outrigger after leveling with five different controllers is closely near the reference value of 77.33 kN, which means all controllers can achieve leveling control and verify the effectiveness of the control method indirectly. From 0 to 2 s, the increase rates of the four outriggers' maximum load based on SLCM-VLC are 2.46%, 10.00%, 5.34%, and 9.84%, which are substantially lower than the maximum increase in the other controllers, suppressing the load fluctuation significantly. Subsequently, from 2 s to 8 s, it can be found that the maximum loads of outriggers 1 and 3 are 81.44 kN and 83.21 kN among the five controllers, corresponding to change rates of 5.46%

and 7.49%, respectively. Notably, the maximum load fluctuations of the four outriggers with SLCM-VLC are the smallest, which are 2.16% and 3.86%, respectively. As a result, it can be calculated that the maximum load fluctuations of outriggers 1 and 3 are reduced by 60.4% and 48.5% based on SLCM-VLC, compared with the maximum outrigger load of the other four strategies. Meanwhile, compared with the SLCM-VLC (T-S), the load suppression performance is further improved (maximum reduction is 1.7%) without load oscillation, and the platform stability is further enhanced. These results demonstrate that the spatial differentiation effect caused by the inclination angle are effectively mitigated with the proposed SLCM-VLC, achieving dynamic load suppression.

Table 4. Load data in simulation on the flat road.

Outrigger	Controller	Static Outrigger Load (kN)	Time (s)			
			0–2 s		2–8 s	
			Maximum Outrigger Load (kN)	Maximum Outrigger Load Fluctuation	Maximum Outrigger Load (kN)	Maximum Outrigger Load Fluctuation
Outrigger 1	PID-CC	77.30	80.86	4.61%	81.15	4.98%
	MPC-CC	77.22	79.72	3.23%	81.44	5.46%
	SLCM-VLC (Q = 0.5)	77.32	79.33	2.59%	80.73	4.41%
	SLCM-VLC (T-S)	77.15	79.26	2.73%	80.09	3.81%
	SLCM-VLC	77.42	79.33	2.46%	79.10	2.16%
Outrigger 2	PID-CC	77.28	88.71	14.79%	79.89	3.38%
	MPC-CC	77.36	86.34	11.60%	77.44	0.09%
	SLCM-VLC (Q = 0.5)	77.26	85.33	10.45%	78.27	1.30%
	SLCM-VLC (T-S)	77.15	84.91	10.06%	78.74	2.05%
	SLCM-VLC	77.16	84.88	10.00%	79.05	2.44%
Outrigger 3	PID-CC	77.50	82.20	6.06%	82.92	6.99%
	MPC-CC	77.41	81.83	5.70%	83.21	7.49%
	SLCM-VLC (Q = 0.5)	77.52	81.77	5.49%	82.01	5.80%
	SLCM-VLC (T-S)	77.15	81.75	5.96%	81.44	5.56%
	SLCM-VLC	77.62	81.76	5.34%	80.61	3.86%
Outrigger 4	PID-CC	77.25	88.86	15.04%	80.08	3.67%
	MPC-CC	77.33	86.03	11.25%	77.59	0.34%
	SLCM-VLC (Q = 0.5)	77.23	85.24	10.38%	78.37	1.48%
	SLCM-VLC (T-S)	77.15	84.59	9.64%	78.79	2.12%
	SLCM-VLC	77.13	84.72	9.84%	79.05	2.50%

The speed diagram of the four outriggers is presented in Figure 11. From 0.5 s to 0.7 s, smaller overshoot and faster initial convergence speed are exhibited with the control of SLCM-VLC compared with the traditional control method (MPC-CC, PID-CC), exhibiting excellent dynamic response performance. Moreover, it can be seen that the output of speed responds to the changes under force constraint after 2 s, owing to the load constraint designed in the SLCM-VLC. Notedly, unlike the T-S fuzzy control that relies on the exact model, the proposed method performs better in response speed compared to the SLCM-VLC(T-S); this advantage stems from the lower computational complexity and efficient reasoning mechanism of the in-built fuzzy controller, which can quickly adapt to dynamic changes. Table 5 displays the detail speed data during the start-up phase from 0 to 2 s, corresponding to Figure 11.

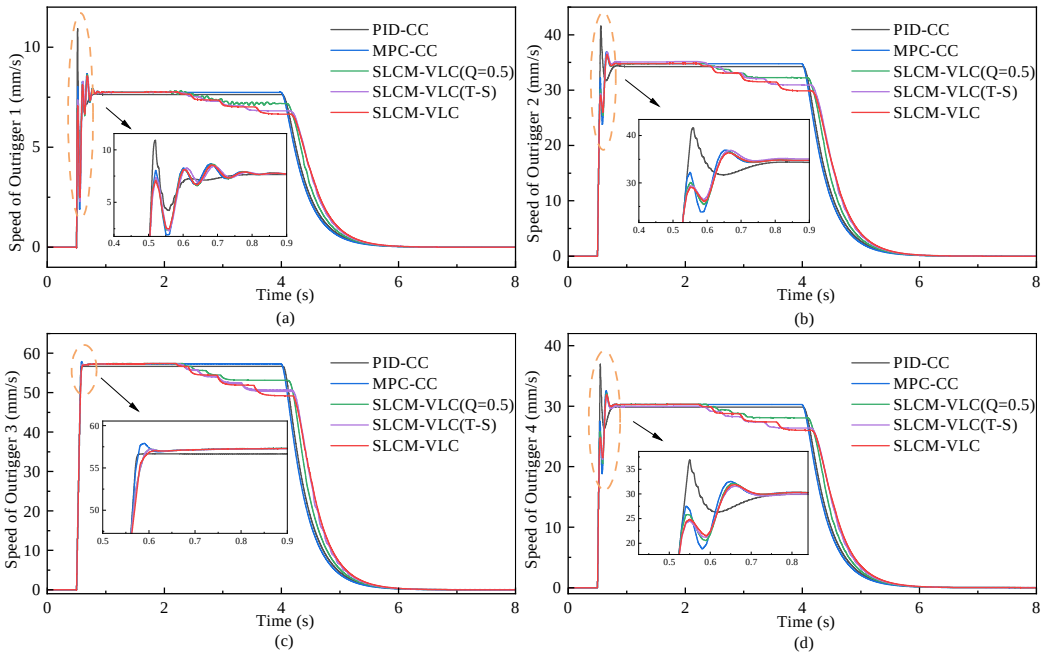


Figure 11. Speed of each outrigger: (**a**) outrigger 1; (**b**) outrigger 2; (**c**) outrigger 3; (**d**) outrigger 4.

Table 5. Speed data for each outrigger from 0 to 2 s.

Outrigger	Controller	Steady State Value (mm/s)	Peak Value (mm/s) (0–2 s)	Overshoot (%) (0–2 s)
Outrigger 1	PID-CC	7.63	10.92	43.11%
	MPC-CC	7.74	8.68	12.02%
	SLCM-VLC (Q = 0.5)	7.77	8.64	11.07%
	SLCM-VLC (T-S)	7.74	8.47	9.42%
	SLCM-VLC	7.76	8.55	10.27%
Outrigger 2	PID-CC	34.27	41.63	21.49%
	MPC-CC	34.78	36.93	6.18%
	SLCM-VLC (Q = 0.5)	34.82	36.53	4.92%
	SLCM-VLC (T-S)	35.12	36.88	5.01%
	SLCM-VLC	34.82	36.34	4.38%
Outrigger 3	PID-CC	56.66	56.73	0.13%
	MPC-CC	57.31	57.91	1.06%
	SLCM-VLC (Q = 0.5)	57.38	57.44	0.10%
	SLCM-VLC (T-S)	57.35	57.37	0.04%
	SLCM-VLC	57.39	57.40	0.02%
Outrigger 4	PID-CC	29.84	36.93	23.77%
	MPC-CC	30.27	32.54	7.49%
	SLCM-VLC (Q = 0.5)	30.31	32.11	5.95%
	SLCM-VLC (T-S)	29.95	31.59	5.48%
	SLCM-VLC	30.31	31.89	5.22%

As shown in Table 5, compared with the PID-CC method, the overshoot suppression effect of SLCM-VLC is particularly prominent. The overshoot of the four outriggers decreases by 32.84%, 17.11%, 0.11%, and 18.55%, respectively, through the application of SLCM-VLC, which significantly improves the performance of overshoot suppression. The speed overshoot of each outrigger is reduced by approximately 2% compared with the MPC-CC algorithm. At the same time, compared with SLCM-VLC under fixed weight, the proposed method also has an improvement of about 0.5% of the overshoot. At the same time, compared with the SLCM-VLC under fixed weight and the SLCM-VLC of the T-S

type, the proposed method also has improvements of about 0.5% and 0.2% of the overshoot, respectively. The above improvements are attributed to the decision optimization based on the MPC framework and innovative introduction of the dynamic load constraint mechanism in the SLCM-VLC, which solves the outrigger impact problem caused by the ignoring of load limitations in existing methods.

Figure 12 illustrates the power variation during the operation of each outrigger. At the beginning of start-up, substantial power is required by each controller to counteract the gravitational potential energy imposed by the crane on the outrigger. Notably, high instantaneous power is exhibited by the PID-CC, which may affect the safety of the controller. During the leveling process, the proposed SLCM-VCL (including fixed weight and T-S type) consistently consumes less power than the MPC-CC. After 2 s, the proposed SLCM-VCL shows a clear reduction in required power and no oscillation compared with fixed-weight and T-S types. These observations align with the results in Figures 10 and 11, indicating that the position–force mechanism in the DFCC is activated, and the change in the weight Q generated by the fuzzy controller is stable. These results show that the proposed SLCM-VCL not only ensures position–force coordination but also produces lower and stable power requirements.

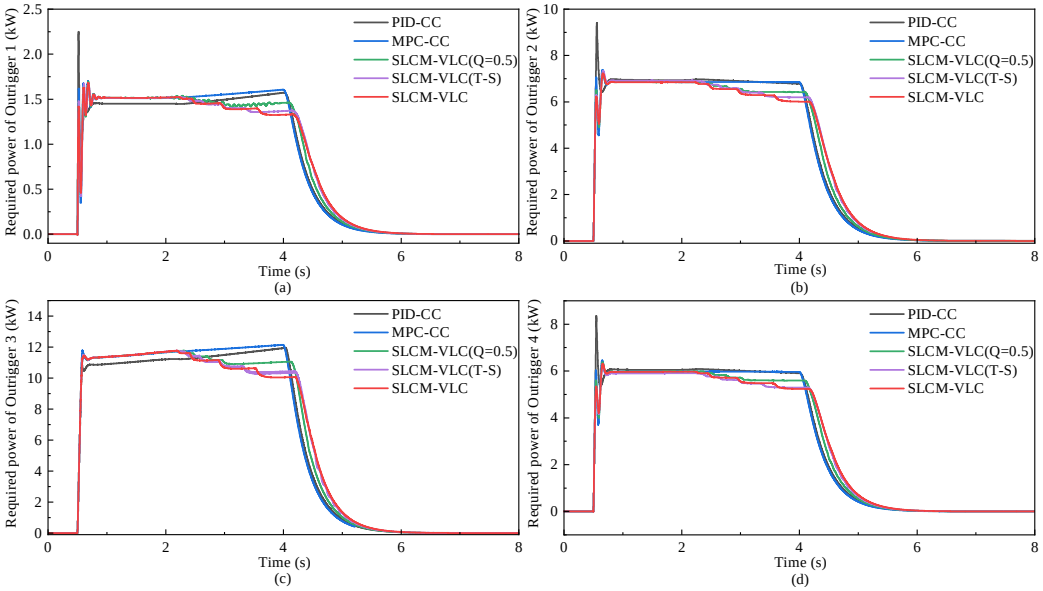


Figure 12. Required power of each outrigger on the flat road: (**a**) outrigger 1; (**b**) outrigger 2; (**c**) outrigger 3; (**d**) outrigger 4.

4.2.2. Analysis of Simulation Results on the Undulating Road

The pitch angle and roll angle of the vehicle platform during the leveling process in working condition 2 are shown in Figure 13. Owing to the increase in inclination angle, it can be seen that the leveling time of the proposed SLCM-VLC increases accordingly. Figure 13a,b indicate that the pitch angle and roll angle of the vehicle are controlled within the safe range of 0.1° within 8 s and 7.52 s, respectively. Finally, both of the angles are further converged to approximately 0°, and it can be concluded that the proposed SLCM-VLC method can achieve high-precision synchronous leveling on complex undulating road within a relatively short time.

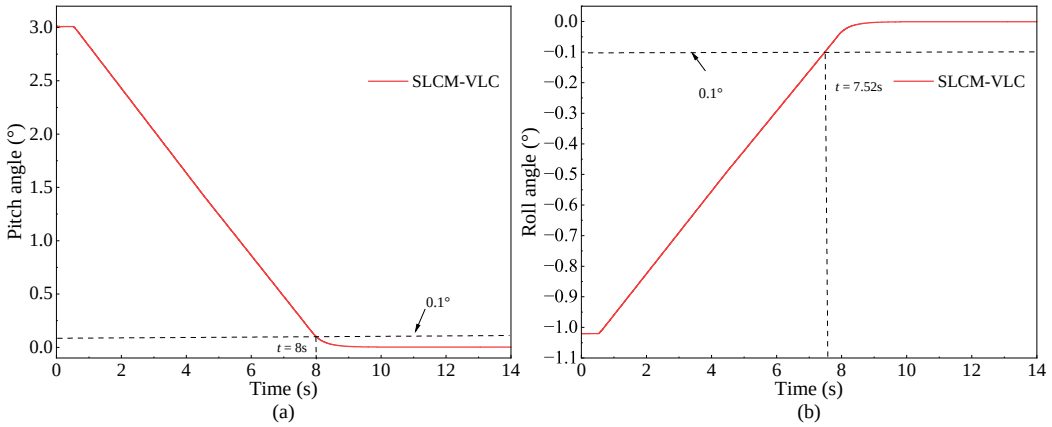


Figure 13. Position of vehicle platform on the undulating road: (**a**) pitch angle variation; (**b**) roll angle variation.

According to the initial inclination angle, it can be found that the outrigger 3 is the lowest point and the outrigger 1 is the highest point. The greater inclination results in a more significant difference in the load distribution among the outriggers. Figures 14 and 15 are the relative synchronization error and load variation in each outrigger under this condition. Within the period from 0 s to 1 s, it can be seen that sudden increase in synchronization errors and the load of the outriggers are caused by the huge impact at the start of the leveling. At the same time, it can be seen that the synchronization errors of the five controllers are close at 0.25%, but the PID-CC controller is more sensitive to the huge impact, resulting in a relatively lagging convergence speed compared to the other five controllers. When the other controllers achieve completed error convergence within 0.8 s, the PID-CC is still at an error state of 0.1% with a slow convergence speed. It leads to the maximum initial load of the PID-CC being different among the four outriggers before leveling, with the maximum load difference reaching 17 kN (outrigger 1 and outrigger 2), which is much higher than the other four controllers.

From 4 s to 9 s, it can be seen that the synchronization error fluctuates under the SLCM-VLC controller compared with the others, whose maximum value is 0.14%. Correspondingly, the loads of outrigger 1 and outrigger 3 decrease by 1.21 kN and 1.91 kN compared to the maximum load, owing to the load constraint in the DFCC being activated. Meanwhile, since the SLCM-VLC method adopts a rule-based regulation mechanism (compared with the T-S), the variation range of the weight parameters is relatively small, thereby effectively suppressing the load fluctuations. It indicates that the proposed SLCM-VLC can achieve effective coordination and optimization of displacement–force even under the undulating road.

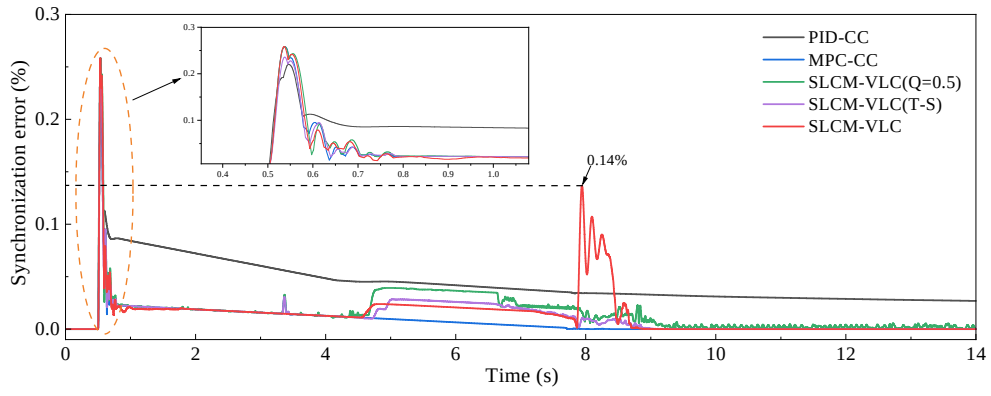


Figure 14. Relative synchronization error under different controllers on the undulating road.

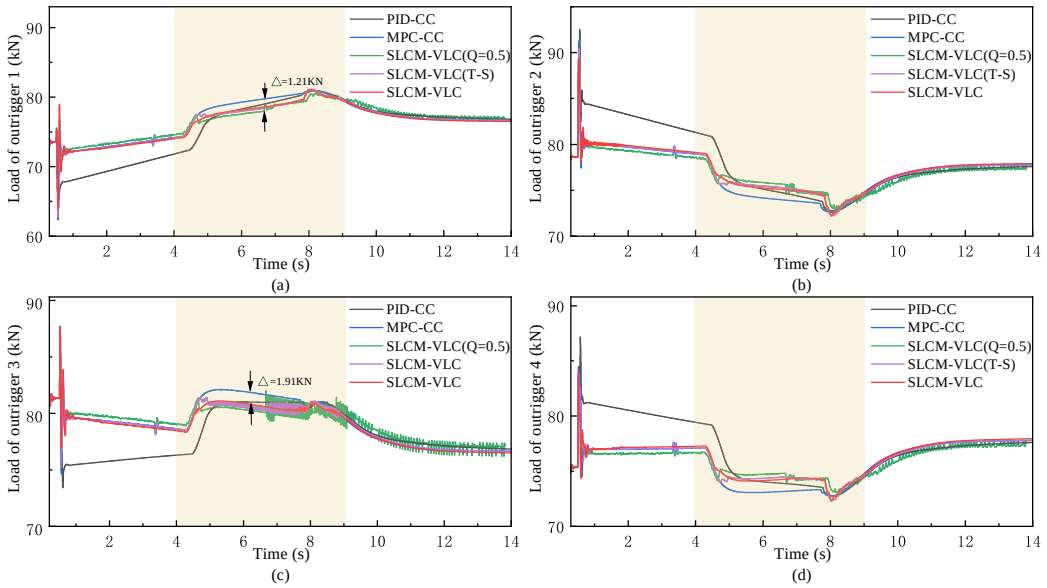


Figure 15. Load variations of each outrigger on the undulating road: (**a**) outrigger 1; (**b**) outrigger 2; (**c**) outrigger 3; (**d**) outrigger 4.

Figure 16 shows the power variations during the operation of each outrigger on the undulating road. Due to the increased inclination angle, the required power of the outriggers is enlarged, leading to a more significant power disparity among them. As shown in Figure 16, lower power consumption is required by the SLCM-VCL (including both fixed-weight and T-S types) compared to the PID-CC and MPC-CC. Additionally, power fluctuation is observed in the fixed-weight and T-S types of the SLCM-VCL. In contrast, no fluctuations are generated by the proposed SLCM-VCL, and power demand is further reduced. This indicates that the weight Q, which is produced by the fuzzy controller, varies steadily. It is demonstrated that even under the extreme condition of large inclination angles, the proposed SLCM-VCL also can achieve effective position–force coordination while maintaining power characteristics well.

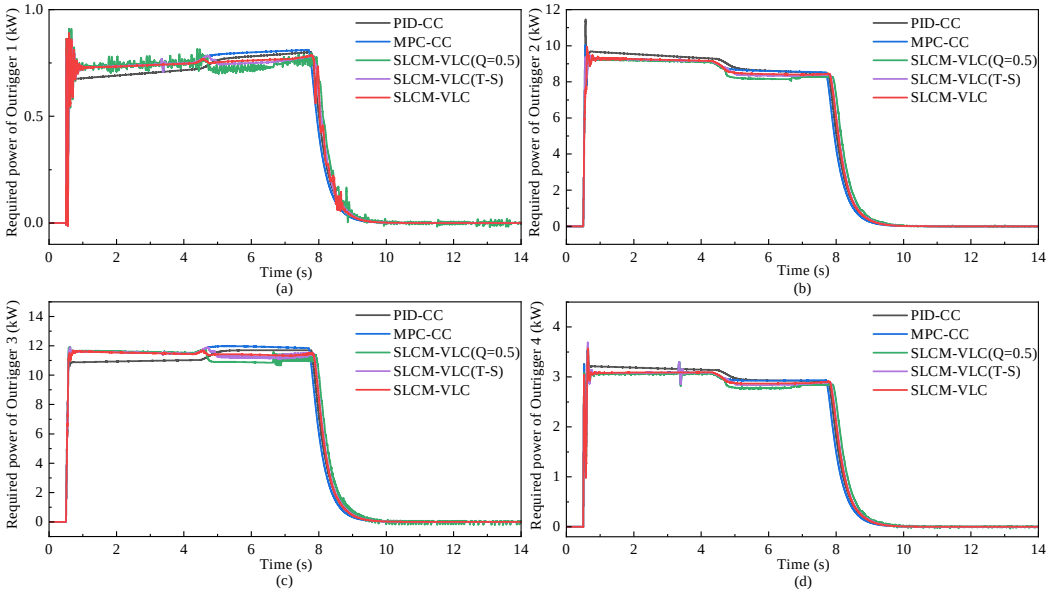


Figure 16. Required power of each outrigger on undulating road: (**a**) outrigger 1; (**b**) outrigger 2; (**c**) outrigger 3; (**d**) outrigger 4.

5. Conclusions

Aiming to achieve synchronous leveling of the crane outrigger platform with small peak load, a synchronous leveling control method with variable load constraints (SLCM-VLC) is proposed in this paper, which integrates the decision optimization of MPC, the nonlinear processing of fuzzy control, and the interference compensation of ESO. Based on the proposed strategy, a dynamic balance synchronization of the outrigger platforms is achieved with consideration of load constraints and compensation for model uncertainties and external disturbances. Meanwhile, for the purpose of validating the underlying logic and the reliability of the design approach, co-simulation and analysis verification based on Matlab, Soildworks, and Adams are carried out and have shown that the controller with the designed strategy is obviously better than the others. The simulation results proved the proposed SLCM-VLC can ensure high-precision leveling while reducing the maximum load and required power of the outriggers. For instance, the synchronous leveling of the vehicle is achieved with small synchronization error of the outriggers <1% and body angle $\leq 0.1^\circ$ through the proposed SLCM-VLC on the flat road, improving the leveling precision compared with the other control strategies. At the same time, while reducing the load oscillation of the outriggers, the maximum load of the main bearing force outrigger is significantly reduced by 3.13% via introducing the variable weight load constraint strategy under rule regulation, which effectively improves the structural safety. Furthermore, the dynamic performance of the electric cylinder motor is optimized synchronously, whose overshoot is reduced by about 2% and the convergence speed is improved by the SLCM-VLC while reducing the required power.

The method's efficacy has been validated by the above results, and it is important to acknowledge the limitations of the model and proposed method. For example, the model of the outrigger platform relied primarily on mathematical formulations that may not fully capture physical nonlinearities. Moreover, there is control error accumulation among the cascaded controllers of the SLCM-VLC, which affects the leveling accuracy and speed. In the future, our research will focus on exploring these limitations while considering factors such as structural elastic deformation and control delay on leveling control and completing the physical experiment, thereby achieving more extensive and effective technological advancements.

Author Contributions: Conceptualization, F.X.; methodology, F.X.; software, H.H.; validation, H.H. and S.F.; formal analysis, S.F.; investigation, F.X.; resources, F.X.; data curation, C.Z.; writing—original draft preparation, H.H.; writing—review and editing, C.Z.; supervision, C.Z.; project administration, F.X.; funding acquisition, F.X. and C.Z. All authors have read and agreed to the published version of the manuscript.

Funding: This work was supported in part by the National Key Research and Development Program under Grant 2023YFC2907600, in part by the National Natural Science Foundation of China under Grant 52475143, in part by the Jiangsu Provincial Natural Science Foundation (BK20241638), in part by the Open Foundation of the State Key Laboratory of Fluid Power and Mechatronic Systems under Grant GZKF-202421, and in part by the Guangdong Basic and Applied Basic Research Foundation under Grant 2024A1515110216.

Data Availability Statement: The data presented in this paper are available from the corresponding author upon request.

Conflicts of Interest: The authors declare no conflicts of interest.

References

1. Zhu, A.; Zhang, Z.; Pan, W. Technologies, levels and directions of crane-lift automation in construction. *Autom. Constr.* **2023**, *153*, 104960. [CrossRef]
2. Ramli, L.; Mohamed, Z.; Abdullahi, A.M.; Jaafar, H.I.; Lazim, I.M. Control strategies for crane systems: A comprehensive review. *Mech. Syst. Signal Proc.* **2017**, *95*, 1–23. [CrossRef]
3. Wu, R.; Liu, X.; Chen, T.; Sun, L.; Wang, N. Almost Disturbance Decoupling Control Strategy for a Class of Underactuated Nonlinear Systems with Disturbances. *Actuators* **2025**, *14*, 56. [CrossRef]
4. Nie, Z.; Wang, H.; Lu, B.; Zhang, F.; Wang, M.; Wu, Z.; Gang, X.; Li, L. Development and first test of an attitude and load coupling adjustment chassis for aerial working platforms. *Mech. Based Des. Struct. Mech.* **2024**, *52*, 2066–2084. [CrossRef]
5. Liang, D.; Chen, S.H.; Chen, Z.; Wu, Y.; Chu, L.Y.; Xue, F. 4D point cloud-based spatial-temporal semantic registration for monitoring mobile crane construction activities. *Autom. Constr.* **2024**, *165*, 105576. [CrossRef]
6. Wang, G.; Qu, W.; Chen, C.; Chen, Z.; Fang, Y. A road level identification method for all-terrain crane based on Support Vector Machine. *Measurement* **2022**, *187*, 110319. [CrossRef]
7. Ji, S.; Li, W.; Zhang, B.; Ji, W.; Wang, Y.; Ng, S.-K. Multivariate Prediction Soft Sensor Model for Truck Cranes Based on Graph Convolutional Network and Random Forest. *Actuators* **2024**, *13*, 357. [CrossRef]
8. Sun, X.Q.; Cai, Y.F.; Yuan, C.C.; Wang, S.H.; Chen, L. Fuzzy sliding mode control for the vehicle height and leveling adjustment system of an electronic air suspension. *Chin. J. Mech. Eng.* **2018**, *31*, 25. [CrossRef]
9. Li, X.; Ruan, P.; Hao, W.; Xie, M.; Lv, T. Modeling and analysis of electromechanical automatic leveling mechanism for high-mobility vehicle-mounted theodolites. *IEICE Trans. Fundam. Electron. Commun. Comput. Sci.* **2024**, *107*, 1027–1039. [CrossRef]
10. Zuo, D.; Liu, J.; Ma, G.; Cao, Y.; Ye, T.; Zhou, B. Fuzzy PID synchronous leveling system coupled with sync-drive for hydraulic outriggers of CBP: Co-simulation and experimental verification. *Mech. Based Des. Struct. Mech.* **2024**, *52*, 5536–5561. [CrossRef]
11. Cai, J.; Ji, Y.; Rong, Z.; Gang, X.; Zhang, F. Geometry-leveling and load-uniforming coupling control for the hyperstatic-outriggerged platform by modeling its inherent properties. *Appl. Optics* **2024**, *63*, 7453–7464. [CrossRef]
12. Zhang, S.; He, X.; Zhu, H.; Li, X.; Liu, X. PID-like coupling control of underactuated overhead cranes with input constraints. *Mech. Syst. Signal Proc.* **2022**, *178*, 109274. [CrossRef]
13. Kwiatoń, P.; Cekus, D.; Waryś, P. Computer-aided rotary crane stability assessment. *Autom. Constr.* **2024**, *162*, 105370. [CrossRef]
14. Wang, Z.; Xia, Y. Model establishment of body attitude adjustment system based on Backstepping control algorithm and automatic leveling technology. *Cluster Comput.* **2019**, *22*, 14327–14337. [CrossRef]
15. Wu, Z.; Zhang, F.; Nie, Z.; Cai, J.; Li, C. Experimental comparison of leveling control schemes for the hyperstatic-outrigger support platform. *Proc. Inst. Mech. Eng. Part C-J. Eng. Mech. Eng. Sci.* **2024**, *238*, 6290–6303. [CrossRef]
16. Li, G.; Ma, X.; Yang, L.; Li, J.; Tian, J.; Li, Y. Adaptive output feedback anti-swing control for underactuated 7-DOF rotary crane with gravitational estimation. *Mech. Syst. Signal Proc.* **2025**, *229*, 112495. [CrossRef]
17. Yeon, H.; Umemoto, K.; Shimizu, S.; Endo, T.; Matsuno, F.; Mizuki, K. Control system design for a class of non-cascade nonlinear under-actuated systems with an application to a rotary crane system. *Mechatronics* **2023**, *96*, 103087. [CrossRef]
18. Yang, W.; Zhang, F.; Wang, H.; Wu, J.; Nie, Z.; Li, L. Synchronous control theory and first test of time-varying upper operation and chassis attitude maintenance for truck cranes. *J. Constr. Eng. Manag.* **2023**, *149*, 04022156. [CrossRef]
19. Yang, T.; Chen, H.; Sun, N.; Fang, Y. Adaptive neural network output feedback control of uncertain underactuated systems with actuated and unactuated state constraints. *IEEE Trans. Syst. Man Cybern.* **2021**, *52*, 7027–7043. [CrossRef]
20. Precup, R.E.; Nguyen, A.T.; Blažič, S. A survey on fuzzy control for mechatronics applications. *Int. J. Syst. Sci.* **2024**, *55*, 771–813. [CrossRef]
21. Hentout, A.; Maoudj, A.; Kouider, A. Shortest path planning and efficient fuzzy logic control of mobile robots in indoor static and dynamic environments. *Sci. Technol.* **2024**, *27*, 21–36. [CrossRef]
22. Li, S.; Zhou, Y.; Ou, D.; Wang, W. Research on Electromechanical Four-Point Leveling Control System Based on MPC. *Front. Mech. Eng.* **2020**, *2*, 20–24. [CrossRef]
23. Liu, A.; Wu, J.; Zhang, F.; Yang, W.; Wang, H. Studies on a statically determinate leveling control strategy for a statically indeterminate four-outrigger support vehicle-borne platform. *Mech. Based Des. Struct. Mech.* **2023**, *51*, 7131–7148. [CrossRef]
24. Shen, J.; Wang, X.; Xiao, D.; Wang, Z.; Mao, Y.; He, M. Online switching strategy between dual three-phase PMSM and open-winding PMSM. *IEEE Trans. Transp. Electrif.* **2023**, *10*, 1519–1529. [CrossRef]
25. Zhang, X.; Wu, Z. Two-Stage Model Predictive Current Control for PMSM Drives With Parameter Robustness Improvement. *IEEE Trans. Energy Convers.* **2023**, *39*, 1352–1360. [CrossRef]
26. Wen, J.; Wang, F. Stable levitation of single-point levitation systems for maglev trains by improved cascade control. *Rom. J. Inf. Sci. Technol.* **2024**, *27*, 348–361. [CrossRef]

Disclaimer/Publisher's Note: The statements, opinions and data contained in all publications are solely those of the individual author(s) and contributor(s) and not of MDPI and/or the editor(s). MDPI and/or the editor(s) disclaim responsibility for any injury to people or property resulting from any ideas, methods, instructions or products referred to in the content.